Nanoscale

RSC Publishing

PAPER

View Article Online
View Journal | View Issue

Published on 19 August 2013. Downloaded by University of California - Santa Cruz on 18/10/2013 18:22:56.

Cite this: *Nanoscale*, 2013, **5**, 10283

High power density microbial fuel cell with flexible 3D graphene–nickel foam as anode†

Hanyu Wang,‡[a] Gongming Wang,‡[a] Yichuan Ling,[a] Fang Qian,[b] Yang Song,[a] Xihong Lu,[ac] Shaowei Chen,[a] Yexiang Tong[c] and Yat Li*[a]

Received 8th July 2013
Accepted 12th August 2013

DOI: 10.1039/c3nr03487a

www.rsc.org/nanoscale

The structure and electrical conductivity of anode play a significant role in the power generation of microbial fuel cells (MFCs). In this study, we developed a three-dimensional (3D) reduced graphene oxide–nickel (denoted as rGO–Ni) foam as an anode for MFC through controlled deposition of rGO sheets onto the nickel foam substrate. The loading amount of rGO sheets and electrode surface area can be controlled by the number of rGO loading cycles. 3D rGO–Ni foam anode provides not only a large accessible surface area for microbial colonization and electron mediators, but also a uniform macro-porous scaffold for effective mass diffusion of the culture medium. Significantly, at a steady state of the power generation, the MFC device with flexible rGO–Ni electrodes produced an optimal volumetric power density of 661 W m^{-3} calculated based on the volume of anode material, or 27 W m^{-3} based on the volume of the anode chamber. These values are substantially higher than that of plain nickel foam, and other conventional carbon based electrodes (*e.g.*, carbon cloth, carbon felt, and carbon paper) measured in the same conditions. To our knowledge, this is the highest volumetric power density reported for mL-scale MFC device with a pure strain of *Shewanella oneidensis* MR-1. We also demonstrated that the MFC device can be operated effectively in a batch-mode at least for a week. These new 3D rGO–Ni electrodes show great promise for improving the power generation of MFC devices.

Introduction

Microbial fuel cells (MFCs) employ electrogenic bacteria to recover chemical energy stored in biodegradable organic materials to electrical energy *via* a bio-oxidation process, which holds great potential for simultaneously addressing the needs for energy regeneration and organic waste treatment.[1–6] However, the relatively low power output of MFCs restricts their practical application. A number of methods have been used in improving MFC power output, including optimization of microbial activities[7,8] and MFC device configuration,[9–12] activation of cathode electrode by incorporating various catalysts such as Au,[13–15] Pd,[16,17] and Ni,[18,19] as well as enhancement of effective surface area of both anode[20–22] and cathode.[23,24] The rapid advancement of nanostructured electrodes opens up new opportunities in the development of high performance MFCs.

Carbon-based materials such as carbon cloth, carbon paper, carbon felt and graphite brush are most commonly used anode materials for MFCs.[25] These commercially available electrode materials are chemically inert, highly conductive and inexpensive. However, these microstructures have a relatively small surface area for bacterial colonization, and thus, limit the power density of MFC device. Previous studies have demonstrated that the power density of MFC can be enhanced by modifying the electrodes with nanostructures to increase the accessible surface area for bacterial colonization. For example, carbon electrodes modified with Au and Pd nanoparticles shown improved power densities.[26] Roh *et al.* reported that the power density of carbon paper was improved by decorating it with multi-walled carbon nanotube/polyarcylonitrile composite.[27] To further improve the performance of the anode, 3D structures with a potentially larger surface area are emerging as new electrode materials for MFCs. For instance, Higgins *et al.* reported the preparation of 3D chitosan–carbon nanotube scaffolds, with a pore size distribution between 10 and 120 μm, as MFC anode.[28] Xie *et al.* reported the fabrication of single-walled carbon nanotubes and graphene-coated textile[29] and sponge[30,31] bio-electrodes for MFCs. Recently, Yong *et al.* developed a 3D conducting graphene–polyaniline scaffold as MFC anode.[20] These MFC devices with 3D electrodes showe a significantly enhanced power output and suggest the potential of 3D conducting scaffold for MFC electrodes.

[a]*Department of Chemistry and Biochemistry, University of California, Santa Cruz, California 95064, USA. E-mail: yli@chemistry.ucsc.edu*

[b]*Physical and Life Sciences Directorate, Lawrence Livermore National Laboratory, California 94550, USA*

[c]*KLGHEI of Environment and Energy Chemistry, MOE of the Key Laboratory of Bioinorganic and Synthetic Chemistry, School of Chemistry and Chemical Engineering, Sun Yat-Sen University, Guangzhou 510275, People's Republic of China*

† Electronic supplementary information (ESI) available. See DOI: 10.1039/c3nr03487a

‡ These authors contributed equally to this work.

Published on 19 August 2013. Downloaded by University of California - Santa Cruz on 18/10/2013 18:22:56.

Here, we report on the fabrication of a flexible and high performance MFC anode by employing nickel foam as a 3D conducting scaffold and coated with reduced graphene oxide (rGO) sheets to increase its accessible surface area for bacteria colonization and electron mediators. Significantly, the rGO–nickel foam (denoted as rGO–Ni) anode produced a remarkable volumetric power density of 661 W m^{-3} (27 W m^{-3}) at a stable state of power generation, calculated based on the volume of the anode material (based on the anode chamber volume). These values are substantially higher than that of plain nickel foam, and conventional carbon based electrodes (*e.g.*, carbon cloth, carbon felt and carbon paper) electrodes measured in the same conditions.

Experimental

Preparation of graphene oxide (GO)

GO was prepared from graphite powder using Hummer's method. Graphite powder (0.5 g) was mixed with 23 mL concentrated H_2SO_4 and 10 mL concentrated HNO_3 in a container that was cooled in an ice bath. $KMnO_4$ (3 g) was slowly added to the mixture. After the addition of $KMnO_4$, the solution was heated at 35 °C for 3 h, and then diluted with 40 mL of deionized water. After 12 h, the solution was further diluted by adding an additional 200 mL of deionized water, followed by slow addition of 3.0 mL of H_2O_2 (30% v/v). The solution with black graphite suspension was gradually converted into a bright yellow graphite oxide solution. The precipitate of graphite oxide was isolated by centrifugation at 1500 rpm for 30 min, and washed with deionized water, and then re-suspended in 500 mL deionized water. The concentration of the graphite oxide solution is ~1 mg mL^{-1}. The aqueous graphite oxide solution was vigorously sonicated for 2–4 h to exfoliate stacked graphite oxide sheets into monolayer or multi-layered GO sheets.

Deposition of rGO sheets onto nickel foam

The nickel foam substrate was transferred into an autoclave (with Teflon liner) filled with 25 mL aqueous GO solution. The autoclave was heated at 120 °C for 5 h and allowed to cool down at rt. The yellowish nickel foam substrate turned into black color (covered with rGO sheets). The substrate was then washed with deionized water, and then air-dried. To improve the electrical conductivity of rGO sheets, the rGO–Ni substrate was annealed at 400 °C in hydrogen atmosphere in a home-built quartz tube furnace for 30 min.

Fabrication of MFC anode

rGO–Ni composite anodes were fabricated by attaching a Ti wire (the diameter of Ti wire is 0.25 mm) onto the Ni foam substrate by silver conductive epoxy (Ted Pella. Inc., Redding, CA). Carbon felt (GF-S6, Electrolytica, Inc., Amherst, NY), carbon paper (SGL Group, Germany), and carbon cloth (CC6 Plain, Fuel Cell Earth LLC, Stoneham, MA) electrodes were fabricated by directly attaching a Ti wire onto the carbon-based substrates. The projected areas of all anodes are in the range of 7–10 cm^2. The thickness of rGO–Ni electrodes is 1 mm. The thickness of carbon felt electrodes is 6 mm. The thickness of carbon paper and carbon cloth electrodes is 0.5 mm.

Shewanella oneidensis MR-1 bacterial culture and MFC operation

Shewanella oneidensis MR-1 (ATCC 700550) was cultured in trypticase soy broth (TSB) (BD Biosciences, San Jose, CA) under aerobic conditions at rt for 24 h at 30 °C in an incubator shaker with shaking at 150 rpm. The culture was then transferred to the anode chamber of a dual-chamber MFC (chamber volume is ~25 mL). 25 mL solution of 50 mM ferricyanide in 100 mM phosphate buffer (K_2HPO_4 18.2 g L^{-1}, KH_2PO_4 2.56 g L^{-1}, $K_3Fe(CN)_6$ 15.6 g L^{-1}, pH 7.4) was used as catholyte. The voltage of MFC device across an external resistor (1000 Ω) was monitored using a precision multimeter/data acquisition system (2700, Keithley, OH). When the current dropped to the baseline level, fresh TSB medium was slowly injected into the anode chamber *via* a sterile syringe. The current (I) generated in MFC was calculated according to Ohm's law, $I = V/R$, where V was the voltage and R was the external resistor. The power was then calculated as $P = V \times I$. The power densities were calculated based on the volume of the electrodes or the volume of anode chamber (~25 mL).

Methylene Blue absorption measurement

The initial concentration of the MB aqueous solution was 2 mg L^{-1}. The plain nickel foam and rGO–*X*–Ni composite foams were immersed separately in MB aqueous solution. The solutions were stirred in the dark for 24 h to allow reaching absorption–desorption equilibrium. Then, the substrates were removed from the MB solutions. Absorption spectra were collected for the original and these MB solutions using an ATI Unicam UV4 spectrometer by using a 1 cm quartz cuvette with a resolution of 2 nm.

Electrochemical impedance spectroscopy (EIS)

The electrochemical characterization was carried out on CHI 660D electrochemical station using an impedance-potential technique under whole cell conditions. EIS measurements were conducted in a two-electrode mode by recording the impedance spectrum of the anode as working electrode, with the cathode acting as a counter electrode and reference electrode. The impedance spectra were collected at the open-circuit potential by applying a sine wave (5 mV) at a frequency range from 1000 kHz to 10 mHz. The data was analyzed using ZView by fitting the EIS spectra with an equivalent circuit.

Material characterization

SEM images were collected by a field-emission SEM (Hitachi S-4800 II). XPS analysis was carried out on a RBD upgraded PHI-5000C ESCA system (Perkin-Elmer) using Mg-monochromatic X-ray at a power of 25 W with an X-ray-beam diameter of 10 mm, and a pass energy of 29.35 eV. The pressure of the analyzer chamber was maintained below 5×10^{-8} Pa during the

 This journal is © The Royal Society of Chemistry 2013

Published on 19 August 2013. Downloaded by University of California - Santa Cruz on 18/10/2013 18:22:56.

measurement. The binding energy was calibrated using the C 1s photoelectron peak at 284.6 eV as reference.

Results and discussion

rGO–Ni anodes were prepared by refluxing a nickel foam substrate (45–103, Lyrun New Material) in an aqueous graphene oxide (GO) solution at 120 °C in an autoclave (Fig. 1a), followed by annealing in hydrogen atmosphere at 400 °C (Experimental section). The conversion of GO into rGO by a hydrothermal method has been reported elsewhere.[30] The scanning electron microscopy (SEM) image showed that the nickel foam is a continuous 3D scaffold with a pore size ranging between 100 and 500 μm (Fig. 1b). The large pore size allows bacteria colonization in the inner structure of the 3D electrode and efficient mass transfer of the nutrient. The specific surface area of the nickel foam was estimated to be ~3000 m^2 per cubic meter based on its weight and size of the framework. More importantly, it offers a continuous 3D highly conductive surface for rGO coating. We aimed to increase the accessible surface area for bacteria colonization and electron mediator through controlled loading rGO sheets on the nickel foam. After refluxing the nickel foam in GO solutions for 5 h, its color changed from yellowish silver to black. As shown in Fig. 1c, the entire nickel foam scaffold was covered with rGO sheets. rGO–Ni foams were further reduced in a hydrogen atmosphere at 400 °C in a home-built quartz tube furnace to increase their electrical conductivities. Previous studies have demonstrated that bioelectrons generated from bacteria can be effectively transferred to GO and rGO.[32,33] Therefore, the conductive rGO coating is expected to serve as a good electron transfer layer that could facilitate bacterial colonization and power generation.[34,35] Furthermore, the rGO–Ni foam preserves the excellent mechanical properties of the nickel skeleton. It is flexible and can be bent and folded into various shapes (Fig. 1d), which enables it to fit in different MFC devices. Importantly, we did not observe fragmentation of rGO sheets when it was bent repeatedly, suggesting the affinity between rGO and nickel skeleton is strong and the composite structure is stable. Moreover, we have demonstrated the feasibility to scale up the fabrication of rGO–Ni electrode for large-scale MFC devices. Fig. 1e shows a 25 × 20 cm rGO–Ni foam. The electrode size can be further increased, and it is practically only limited by the size of the container for a refluxing process.

The capability of developing a highly conductive electrode with a large effective surface area is essential to the success of developing a high-performance bioanode. To characterize the chemical nature of rGO coating, core level C 1s X-ray photoelectron spectroscopy (XPS) spectra were collected for the rGO–Ni structures before and after hydrogen reduction. As shown in Fig. S1† (ESI) rGO sheets before hydrogenation showed a broad peak centered at 284.8 eV with a shoulder at a higher binding energy, which suggests the existence of more than one chemical state of carbon.[36] The broad peak was deconvoluted into four peaks. The main peak at 284.7 eV can be attributed to the graphite-like sp^2 hybridized carbon, indicating most carbon atoms are arranged in a honeycomb lattice.[37] The synthetic peak

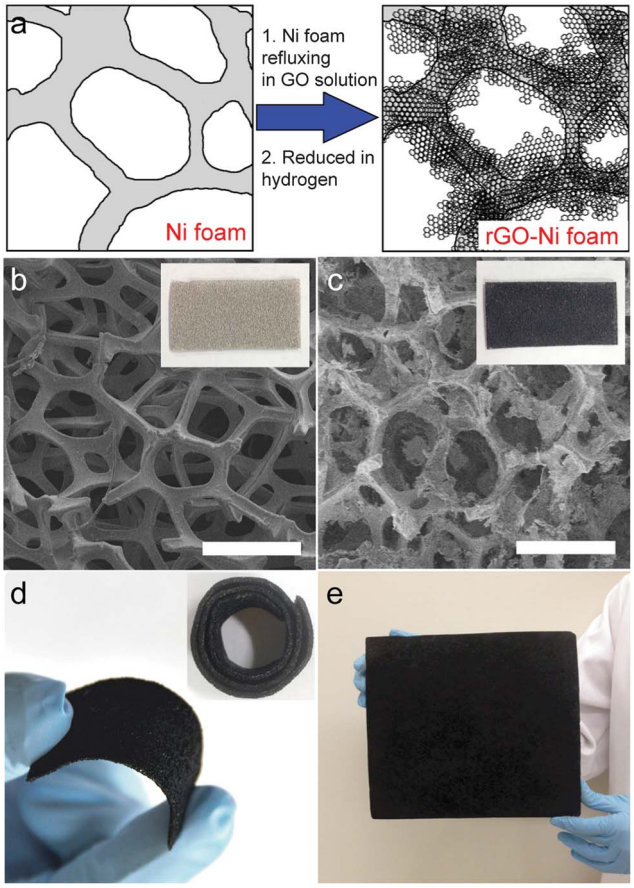

Fig. 1 (a) A schematic diagram illustrates the preparation of rGO–Ni anode. (b and c) SEM images and digital pictures (insets) of plain nickel foam and rGO–Ni foam. Scale bars are 200 μm. (d) Digital picture of a curved rGO–Ni foam. Inset: rGO–Ni foam rolled up into a cylindrical shape. (e) Digital picture of a 25 × 20 cm rGO–Ni foam.

centered at 285.5 eV is consistent with the sp^3 hybridization of C–C or C–H bonds.[38] Small peaks located at the high-energy tail (286.2 eV and 288.9 eV) can be ascribed to the carbon signal in carbon–oxygen compounds such as C–O bond or carboxylate carbon (O–C=O), respectively.[39] Importantly, the intensity of the signals associated with C–O and O–C=O bonds dropped substantially upon hydrogenation, suggesting these surface oxygen containing groups have been reduced.

Moreover, the electrode surface area is expected to be related to the loading amount of rGO sheets, which can be controlled by the number of loading cycles. Nickel foam reflux in GO solution at 120 °C for 5 h is counted as one loading cycle. Fig. 2 shows the SEM images collected for plain nickel foam and rGO–*X*–Ni (*X* = the number of loading cycles) electrodes prepared with a different number of loading cycles. Before loading of rGO sheets, the nickel foam had a smooth surface (Fig. 2a). After refluxing in GO solution, the nickel foam was covered with rGO sheets. The thickness and roughness of rGO coating increased with the number of loading cycles. Furthermore, the amount of rGO loading increased with the number of loading cycles, as expected (Fig. S2, ESI†). It is noteworthy that the deposition of rGO sheets did not significantly change the pore size, and thus,

Published on 19 August 2013. Downloaded by University of California - Santa Cruz on 18/10/2013 18:22:56.

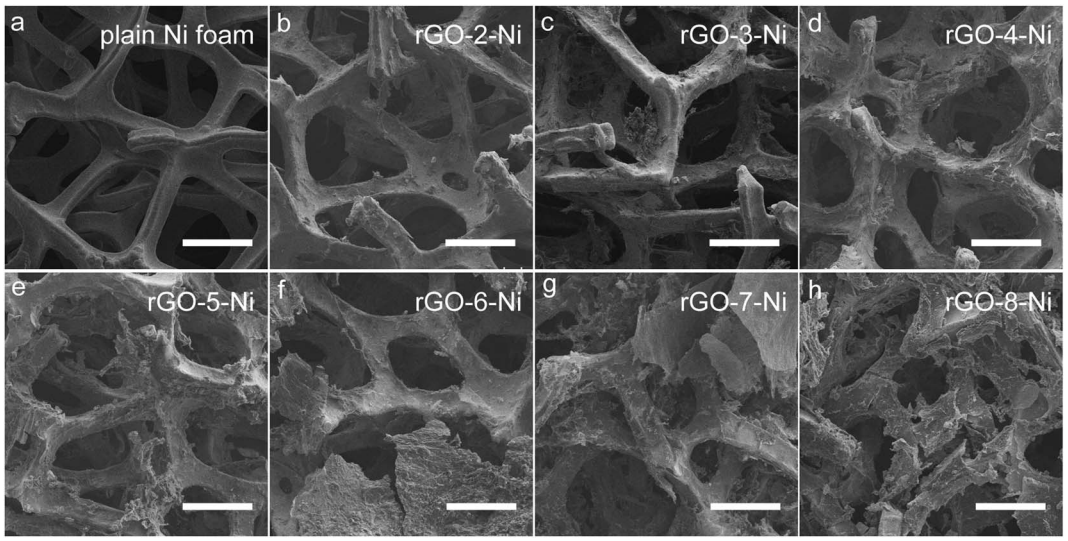

Fig. 2 SEM images of (a) plain nickel foam, and (b–h) rGO–*X*–Ni (*X* = the number of loading cycles) foams. Scale bars are 200 μm.

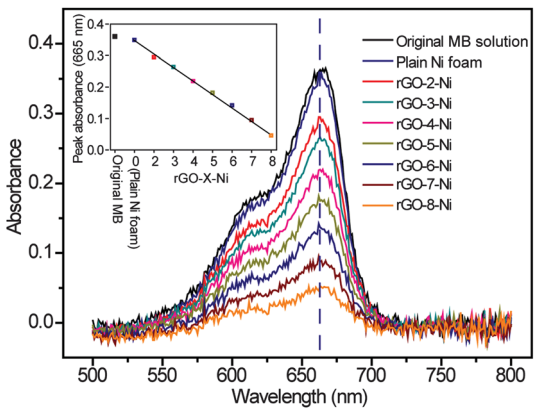

Fig. 3 UV-vis absorption spectra collected for the original MB solution (2 mg L^{-1} in water) and the MB solutions after reacting with rGO–*X*–Ni foams for 24 h. Inset: The absorption peak intensity (665 nm, highlighted by dashed line) of rGO–*X*–Ni foams plot as a function of the number of rGO loading cycles. A line of best-fit by eye was drawn through the data points.

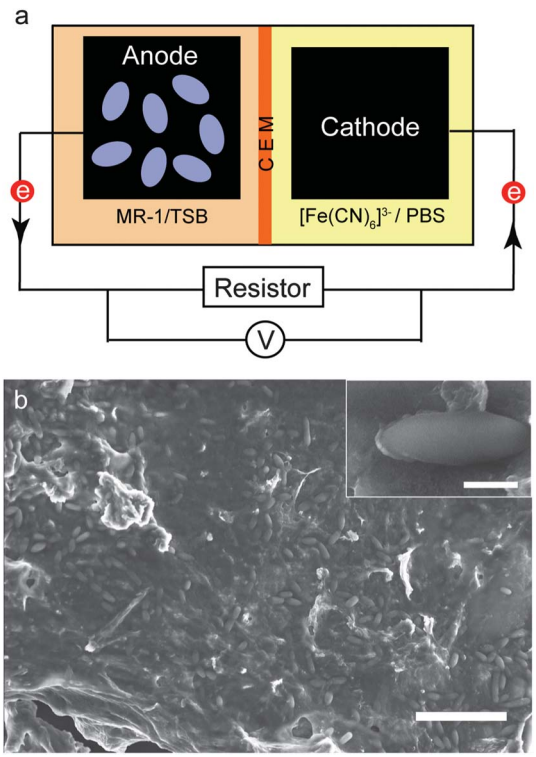

Fig. 4 (a) Schematic diagram illustrating the configuration of a dual-chamber MFC device with MR-1 colonized bioanode and carbon cloth cathode. The anode and cathode chamber were separated by a CEM. MR-1/TSB solution was used as anolyte and ferricyanide/PBS solution was used as catholyte. (b) SEM image of an rGO–Ni anode colonized by rod-shaped *S. oneidensis* MR-1. The scale bar is 20 μm. Inset: magnified SEM image of a MR-1 bacterium. The scale bar is 1 μm.

it seems not likely to affect the mass diffusion of bacterial culture medium. However, we observed that rGO–Ni electrodes became fragile after repeating the loading process for 6 times or more (Fig. S3, ESI†). This could be due to the chemical dissolution of nickel in acidic GO aqueous solution (pH ~ 5).

To test our hypothesis that the effective electrode surface area can be increased by increasing the number of rGO loading cycles, we investigated the surface area for rGO–*X*–Ni structures. Since nickel substrate slowly dissolved in GO solution during the refluxing process, the quantitative determination of the specific surface area for rGO–*X*–Ni electrodes by Brunauer–Emmett–Teller method is impossible. Alternatively, we estimated the surface area of rGO–*X*–Ni electrodes by a dye absorption experiment. Methylene Blue (MB) is a dye that has been widely used for determining the surface area of a solid absorber.[40] The absorption measurements were started with a 2 mg L^{-1} MB^{-1} aqueous solution. The plain nickel foam and rGO–*X*–Ni electrodes were immersed in the MB aqueous solution for 24 h. The solutions were stirred in the dark to establish an adsorption/desorption equilibrium for MB on the electrode surface. UV-vis absorption spectra collected for these solutions

 This journal is © The Royal Society of Chemistry 2013

Published on 19 August 2013. Downloaded by University of California - Santa Cruz on 18/10/2013 18:22:56.

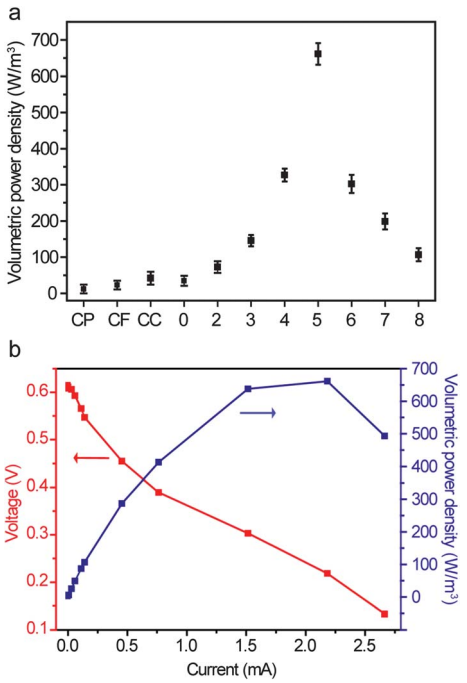

Fig. 5 (a) Maximum volumetric power densities collected for MFC devices with rGO–*X*–Ni electrodes as anodes. Maximum volumetric power densities of MFC devices with plain nickel foam, carbon paper (CP), carbon felt (CF), and carbon cloth (CC) electrodes as anodes are also added for comparison. The error bars show the deviation of the maximum power densities for at least three devices. (b) Polarization and power curves collected for a MFC device with rGO–5–Ni anode.

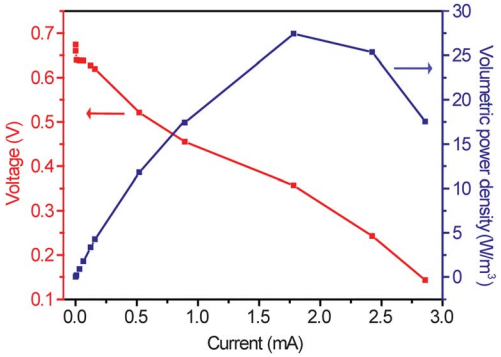

Fig. 6 Polarization (red) and power (blue) curves collected for MFC with rGO–5–Ni anode. The volumetric power densities were calculated based on the volume of the anode chamber (~25 mL).

revealed characteristic absorption peaks of MB (Fig. 3). More importantly, the absorption intensity (665 nm) decreased almost linearly with the increased number of loading cycles (Fig. 3, inset). These results clearly support our hypothesis that the electrode surface area can be increased and controlled by the number of loading cycles.

We investigated the interplay between the performance of rGO–*X*–Ni anode and the number of rGO loading cycles. rGO–*X*–Ni anodes were tested in a conventional, dual-chamber MFC device. The configuration of the MFC device is illustrated in Fig. 4a. The dual-chamber MFC devices were built with glass

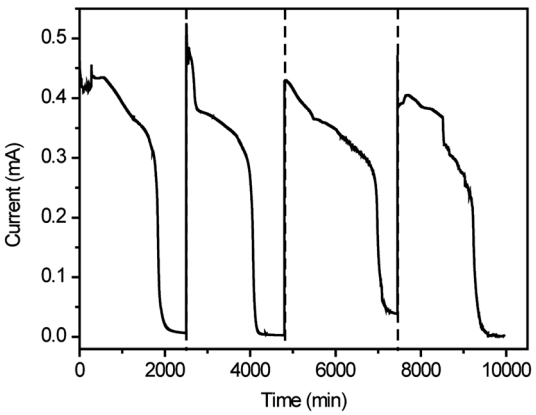

Fig. 7 Current *vs.* time plot collected for a MFC device with rGO–5–Ni anode, operated in a batch-fed mode with an external resistor of 1000 Ω.

tubes jointed by a cation exchange membrane (CEM) (CMI 7000S, Membranes International Inc., Ringwood, NJ, USA). Each chamber had a liquid volume of ~25 mL. In the anode chamber, a pure strain of *Shewanella oneidensis* MR-1 (ATCC 700550) was inoculated in trypticase soy broth (TSB, BD Biosciences, San Jose, CA), which was supplied as growth medium. The cathode chamber was filled with ferricyanide phosphate buffer solution (K_2HPO_4 18.2 g L^{-1}, KH_2PO_4 2.56 g L^{-1}, $K_3Fe(CN)_6$ 15.6 g L^{-1}, pH 7.4). The rGO–*X*–Ni foams with projected areas between 7 and 10 cm^2, and a thickness of 0.1 cm were used as anodes. Carbon cloth substrates (the area of carbon cloth was about 70 cm^2, CC6 Plain, Fuel cell Earth LLC, Stoneham, MA) were used as cathode. An external resistor was connected to the anode and cathode to complete the circuit, and the voltage generated in the MFC was monitored as a function of time. All rGO–*X*–Ni electrodes were measured using the same MFC device to eliminate the possible discrepancy due to device assembly. The MFCs were operated in batch mode at rt (~25 °C). SEM images collected for the bioanode after a few days operation revealed the colonization of MR-1 cells on the rGO sheets and formed a biofilm (Fig. 4b). The magnified SEM image showed that the rod-shaped bacteria have a typical diameter of 0.4–0.9 μm and a length of 2–3 μm, which are consistent with previously reported values for MR-1.

The properties of rGO–*X*–Ni electrodes were investigated through constructing polarization and power curves by varying external resistors between 1 MΩ and 50 Ω. These results were compared to the device using plain nickel foam and conventional anode materials, including carbon felt (GF-S6, Electrolytica, Inc., Amherst, NY), carbon paper (SGL Group, Germany) and carbon cloth (CC6 Plain, Fuel Cell Earth LLC, Stoneham, MA) (Fig. S4, ESI†). Volumetric power densities were calculated based on the volume of the anode electrode when the device established a steady state. Fig. 5a compares the maximum volumetric power densities of MFC devices with different types of anodes. The maximum volumetric power densities of plain nickel foam, carbon felt, carbon paper, and carbon cloth anodes were measured to be 35, 23, 12 and 42 W m^{-3}, respectively. Significantly, MFC devices employing rGO–*X*–Ni

Published on 19 August 2013. Downloaded by University of California - Santa Cruz on 18/10/2013 18:22:56.

composite electrodes as anodes showed substantially higher power densities than the values obtained for these conventional electrodes (Fig. 5a). With the number of rGO loading cycles increasing from 2 to 5 cycles, the maximum power densities of MFC devices were gradually increased from 73 to 661 W m^{-3}. Fig. 5b shows the polarization curve of rGO–5–Ni device. It exhibits an open circuit voltage (OCV) of 0.62 V, comparable to the values reported for other MFC devices with MR-1 colonized as anode.[39] The short-circuit current (2.7 mA) of this device is substantially higher than the values obtained for other anode electrodes we studied. Significantly, the rGO–5–Ni achieved a remarkable volumetric power density of 661 W m^{-3}, which is almost two times higher than the value of a recently reported MFC device with 3D graphene-sponge anode.[31] Moreover, this value is almost 29-fold higher than that of carbon felt, which is a conventional anode material with porous 3D structure. The superior performance of the rGO–5–Ni anode is believed to be due to the increased effective surface area for bacteria and electron mediators, as well as the porous Ni foam scaffold that is highly conductive and allows efficient mass transport of the bacterial culture medium. The maximum power densities of the devices decrease with further increase of the number of loading cycles. One of the possible reasons is the chemical dissolution of nickel resulting in the structural collapse of the nickel skeleton after a prolonged treatment in acidic GO solution during the repeated rGO loading processes. Moreover, rGO sheets tend to form aggregates with the increase of rGO loading cycles (Fig. 2), which could cause decrease of the accessible area for bacteria colonization. Notably, that the MB absorption measurement indicates the surface area increasing continuously with the number of rGO loading cycles, the interior surface in the rGO aggregates may not be accessible for bacteria colonization. Moreover, we also calculate the gravimetric power density of the electrode materials. Since the nickel foam is a 3D structure with a large open space, the gravimetric density of nickel foam ($\sim$0.32 g cm^{-3}) used in this study is indeed comparable to that of carbon cloth ($\sim$0.27 g cm^{-3}), which is another advantage of using a 3D electrode structure for MFC application. In Fig. S5† (ESI), we compare the maximum gravimetric power density of different electrode materials. Again, the gravimetric power densities of nickel foam electrodes are substantially higher than the other carbon materials, and the rGO–5–Ni electrode achieved the highest gravimetric power density. Importantly, these results also indicate that the gravimetric power density of the MFC device could be further improved by replacing the nickel framework with other 3D conductive networks with a lower gravimetric density.

To prove the hypothesis that the 3D conductive scaffold benefits the charge and mass transport, electrochemical impedance spectroscopy (EIS) spectra were also collected and analyzed for conventional carbon cloth anode and rGO–5–Ni anode (Fig. S6, ESI†). By fitting the data of the Nyquist plots with an equivalent circuit, we derived the solution resistance (R_s), charge transfer resistance (R_{p1}) and diffusion resistance (R_{p2}) (Fig. S6b and Table S1, ESI†). As shown in Table S1,† the rGO–5–Ni electrode exhibits considerably smaller resistances than the values obtained on the carbon cloth electrode, especially the diffusion resistance. The rGO–5–Ni anode shows a diffusion resistance of 207 Ω, which is an order of magnitude less than that of carbon cloth electrode (2211 Ω). Since both rGO–5–Ni and carbon cloth anode were measured in the same electrochemical cell and electrolyte, the substantial reduction of resistances can be possibly attributed to the 3D conductive structure that allows efficient electron/mass transport. This study suggests the potential advantage of 3D conductive porous scaffold as electrode for MFC devices.

In previous studies, the volumetric power densities were also calculated based on the volume of the anode chamber.[41] To compare the performance of rGO–*X*–Ni electrodes with these previous results, we fabricated a roll-up rGO–5–Ni electrode (Fig. 1d, inset) that can fit in the 25 mL anode chamber, and measured power and polarization curves for the MFC device (Fig. 6). Moreover, for comparison, power and polarization curves were also collected for MFC devices when the anode chamber was filled with carbon felt or carbon cloth electrodes. Significantly, the maximum volumetric power density of the rGO–5–Ni device was calculated to be 27 W m^{-3}, which is substantially larger than the values obtained for carbon felt (1.03 W m^{-3}) and carbon cloth (1.62 W m^{-3}) anodes (Fig. S7, ESI†) measured with the same MFC device. The power density of 27 W m^{-3} is two orders of magnitude larger than the values reported for other milliliter scale H-shaped MFC devices using graphite sticks as electrodes, and MR-1/lactate–Fe(III) citrate medium (0.25 W m^{-3}) as electrolytes.[42,43] It is 135-fold higher than that of the mL-MFC device with using carbon cloth as anode and MR-1/TSB as anolyte (0.2 W m^{-3}).[44] And it is also almost 6 times higher than that obtained for mL-MFC device with crumpled graphene particles modified carbon cloth anodes (4.8 W m^{-3}) and wastewater as anolyte.[24] To our knowledge, this is the highest volumetric power density obtained for mL-MFC device using a pure strain of MR-1.

To evaluate the stability of rGO–5–Ni anode, the MFC device was operated in a batch mode. Fig. 7 shows the continuous current generation from the MFC device in four consecutive feeding cycles, which lasted for almost a week. In each feeding cycle, a current of 0.1–0.5 mA was generated, which lasted for *ca.* 40 h before decreasing to the baseline due to depletion of the nutrient in the MFC device. The slow decay of the current suggests effective removal of most of the organic matter in the electrolyte. Replenishment of fresh TSB medium into the anode chamber led to drastic current restoration, and bioelectricity generation sustained for another 40 h. After the device operated for $\sim$40 h, the device yielded a coulombic efficiency of 19%, indicating the device efficiently converting organic matter to electricity.[45] The results proved that the MFC device with rGO–5–Ni anode can be operated for at least a week, which is important for practical application.

Conclusion

In summary, we have successfully developed a 3D electrode by coating rGO sheets onto Ni foam for an MFC device. The deposition of rGO sheets on highly conductive Ni foam

 This journal is © The Royal Society of Chemistry 2013

Published on 19 August 2013. Downloaded by University of California - Santa Cruz on 18/10/2013 18:22:56.

considerably increased the effective surface area for microbial colonization. The 3D porous nickel scaffold allows efficient electron transfer and mass transport of bacterial culture medium. MFC devices with rGO–Ni electrodes showed a substantially higher power density output as compared to the device with plain nickel foam and other conventional carbon-based electrodes. In particular, the MFC device with rGO–5–Ni electrode achieved a remarkable volumetric power density of 661 W m^{-3} (based on the volume of the anode) or 28 W m^{-3} (based on the volume of anode chamber), which are the highest values ever obtained for mL-MFCs with a pure strain of *S. oneidensis* MR-1. More importantly, 3D electrode is believed to be a general strategy to improve the power output of MFC devices. The maximum power output reported in this study was still limited by the electron producing capability of pure strain MR-1, and is relatively low as compared to that of other optimized MFC devices with mixed bacteria culture inoculated in wastewater.[46–50] However, we believe a similar enhancement in the power output should be expected for those MFC devices with mixed bacteria culture by using the 3D Ni/rGO anode electrode developed in this study. The demonstration of this new 3D electrode could further push the performance of MFC devices and strongly impact the microbial technology.

Acknowledgements

Y.L. acknowledges financial support from US. NSF (CBET 1034222). F.Q. acknowledges support from LDRD Project 11-LW-054, performed under the auspices of the US. Department of Energy by Lawrence Livermore National Laboratory under Contract DEAC52-07NA27344. S.C. thanks the National Science Foundation (CHE – 1012256 and CBET – 1258839). Y.T.X. acknowledges financial support for this work from the Natural Science Foundation of China (90923008 and 21273290). G.M.W. thanks for financial support from the Chancellor's Dissertation Year Fellowship at University of California, Santa Cruz. X.H.L. thanks the Academic New Artist Ministry of Education Doctoral Post Graduate (China) and the China Scholarship Council for financial support.

References

1 S.-J. Yuan, G.-P. Sheng, W.-W. Li, Z.-Q. Lin, R. J. Zeng and H.-Q. Yu, *Environ. Sci. Technol.*, 2010, **44**, 5575–5580.
2 B. E. Logan, B. Hamelers, R. Rozendal, U. Schroder, J. Keller, S. Freguia, P. Aelterman, W. Verstraete and K. Rabaey, *Environ. Sci. Technol.*, 2006, **40**, 5181–5192.
3 R. S. Berk and J. H. Canfield, *Appl. Microbiol.*, 1964, **12**, 10–12.
4 J. B. Davis and H. F. Yarbrough Jr, *Science*, 1962, **137**, 615–616.
5 S.-J. Yuan, G.-P. Sheng, W.-W. Li, Z.-Q. Lin, R. J. Zeng, Z.-H. Tong and H.-Q. Yu, *Environ. Sci. Technol.*, 2010, **14**, 5575–5580.
6 F. Qian and D. E. Morse, *Trends Biotechnol.*, 2010, **29**, 62–69.
7 H. Liu, S. Cheng and B. E. Logan, *Environ. Sci. Technol.*, 2005, **39**, 5488–5493.
8 J. R. Kim, B. Min and B. E. Logan, *Appl. Microbiol. Biotechnol.*, 2005, **68**, 23–30.
9 X. Zhang, H. Sun, P. Liang, X. Huang, X. Chen and B. E. Logan, *Biosens. Bioelectron.*, 2011, **30**, 267–271.
10 H. Hu, Y. Fan and H. Liu, *Water Res.*, 2008, **42**, 4172–4178.
11 F. Qian, M. Baum, Q. Gu and D. E. Morse, *Lab Chip*, 2009, **9**, 3076–3081.
12 F. Zhang, Z. Ge, J. Grimaud, J. Hurst and Z. He, *Bioresour. Technol.*, 2013, **134**, 251–256.
13 J. Wei, P. Liang and X. Huang, *Bioresour. Technol.*, 2011, **102**, 9335–9344.
14 D. Brondani, E. Zapp, I. C. Vieira, J. Dupont and C. W. Scheeren, *Analyst*, 2011, **136**, 2495–2505.
15 D. Chen, G. Wang and J. Li, *J. Phys. Chem. C*, 2007, **111**, 2351–2367.
16 S. Thiagarajan, R. F. Yang and S. M. Chen, *Bioelectrochemistry*, 2009, **75**, 163–169.
17 X. Wu, F. Zhao, N. Rahunen, J. R. Varcoe, C. Avignone-Rossa, A. E. Thumser and R. C. Slade, *Angew. Chem., Int. Ed.*, 2011, **50**, 427–430.
18 M. Ganesana, G. Istarnboulie, J. L. Marty, T. Noguer and S. Andreescu, *Biosens. Bioelectron.*, 2011, **30**, 43–48.
19 C. W. Welch and R. G. Compton, *Anal. Bioanal. Chem.*, 2006, **384**, 601–619.
20 Y.-C. Yong, X.-C. Dong, M. B. Chan-Park, H. Song and P. Chen, *ACS Nano*, 2012, **6**, 2394–2400.
21 Y. Qiao, S.-J. Bao, C. M. Li, X.-Q. Cui, Z.-S. Lu and J. Guo, *ACS Nano*, 2008, **2**, 113–119.
22 S. Ci, Z. Wen, J. Chen and Z. He, *Electrochem. Commun.*, 2012, **14**, 71–74.
23 T. Zhang, H. Nie, T. S. Bain, H. Lu, M. Cui, O. L. Snoeyenbos-West, A. E. Franks, K. P. Nevin, T. P. Russell and D. R. Lovley, *Energy Environ. Sci.*, 2013, **6**, 217–224.
24 L. Xiao, J. Damien, J. Luo, H. D. Jang, J. Huang and Z. He, *J. Power Sources*, 2012, **208**, 187–192.
25 S.-Q. Ci, N. Wu, Z.-H. Wen and J.-H. Li, *Journal of Electrochemistry*, 2012, **18**, 243–251.
26 Y. Fan, S. Xu, R. Schaller, J. Jiao, F. Chaplen and H. Liu, *Biosens. Bioelectron.*, 2011, **26**, 1908–1912.
27 S.-I. Kim and S.-H. Roh, *J. Nanosci. Nanotechnol.*, 2010, **10**, 3271–3274.
28 S. R. Higgins, D. Foerster, A. Cheung, C. Lau, O. Bretschger, S. D. Minteer, K. Nealson, P. Atanassov and M. J. Cooney, *Enzyme Microb. Technol.*, 2011, **48**, 458–465.
29 X. Xie, L. Hu, M. Pasta, G. F. Wells, D. Kong, C. S. Criddle and Y. Cui, *Nano Lett.*, 2011, **11**, 291–296.
30 X. Xie, M. Ye, L. Hu, N. Liu, J. R. McDonough, W. Chen, H. N. Alshareef, C. S. Criddle and Y. Cui, *Energy Environ. Sci.*, 2012, **5**, 5265–5270.
31 X. Xie, G. Yu, N. Liu, Z. Bao, C. S. Criddle and Y. Cui, *Energy Environ. Sci.*, 2012, **5**, 6862–6866.
32 Y. Yuan, S. zhou, B. Zhao, L. Zhuang and Y. Wang, *Bioresour. Technol.*, 2012, **116**, 453–458.
33 Y.-X. Huang, X.-W. Liu, J.-F. Xie, G.-P. Sheng, G.-Y. Wang, Y.-Y. Zhang, A.-W. Xu and H.-Q. Yu, *Chem. Commun.*, 2011, **47**, 5795.

Published on 19 August 2013. Downloaded by University of California - Santa Cruz on 18/10/2013 18:22:56.

34 K. C. Kemp, H. Seema, M. Saleh, N. H. Le, K. Mahesh, V. Chandra and K. S. Kim, *Nanoscale*, 2013, **5**, 3149–3171.
35 C. Zhu and S. Dong, *Nanoscale*, 2013, **5**, 1753–1767.
36 C. D. Zangmeister, *Chem. Mater.*, 2010, **22**, 5625–5629.
37 R. Lv, Q. Li, A. R. Botello-Mendez, T. Hayashi, B. Wang, A. Berkdemir, Q. Hao, A. L. Elias, R. Cruz-Silva, H. R. Gutierrez, Y. A. Kim, H. Muramatsu, J. Zhu, M. Endo, H. Terrones, J.-C. Charlier, M. Pan and M. Terrones, *Sci. Rep.*, 2012, **2**, 586.
38 S.-K. Jerng, D. S. Yu, J. H. Lee, C. Kim, S. Yoon and S.-H. Chun, *Nanoscale Res. Lett.*, 2011, **6**, 565–570.
39 G. Jo, M. Choe, C.-Y. Cho, J. H. Kim, W. Park, S. Lee, W.-K. Hong, T.-W. Kim, S.-J. Park, B. H. Hong, Y. H. Kahng and T. Lee, *Nanotechnology*, 2010, **21**, 175201–175206.
40 C. Kaewprasit, E. Hequet, N. Abidi and J. P. Gourlot, *J. Cotton Sci.*, 1998, **2**, 164–173.
41 Y. Fan, H. Hu and H. Liu, *J. Power Sources*, 2007, **171**, 348–354.
42 K. P. Nevin, H. Richter, S. F. Covalla, J. P. Johnson, T. L. Woodard, A. L. Orloff, H. Jia, M. Zhang and D. R. Lovley, *Environ. Microbiol.*, 2008, **10**, 2505–2514.
43 M. Lanthier, K. B. Gregory and D. R. Lovley, *FEMS Microbiol. Lett.*, 2008, **278**, 29–35.
44 F. Qian, Z. He, M. P. Thelen and Y. Li, *Bioresour. Technol.*, 2011, **102**, 5836–5840.
45 G. J. Newton, S. Mori, R. Nakamura, K. Hashimoto and K. Watanabe, *Appl. Environ. Microbiol.*, 2009, **75**, 7674–7681.
46 Y. Fan, S.-K. Han and H. Liu, *Energy Environ. Sci.*, 2012, **5**, 8273–8280.
47 Y. Fan, H. Hu and H. Liu, *Environ. Sci. Technol.*, 2007, **41**, 8154–8158.
48 S. Chen, G. He, Q. Liu, F. Harnisch, Y. Zhou, Y. Chen, M. Hanif, S. Wang, X. Peng, H. Hou and U. Schröder, *Energy Environ. Sci.*, 2012, **5**, 9769–9772.
49 S. Chen, H. Hou, F. Harnisch, S. A. Patil, A. A. Carmona-Martinez, S. Agarwal, Y. Zhang, S. Sinha-Ray, A. L. Yarin, A. Greiner and U. Schröder, *Energy Environ. Sci.*, 2011, **4**, 1417–1421.
50 X. Zhang, S. Cheng, P. Liang, X. Huang and B. E. Logan, *Bioresour. Technol.*, 2011, **102**, 372–375.

 This journal is © The Royal Society of Chemistry 2013